Direct Measurement of the Coherence Length of Edge States in the Integer Quantum Hall Regime

Preden Roulleau, F. Portier, and P. Roche
Nanoelectronic group, Service de Physique de l'Etat Condensé, CEA Saclay, F-91191 Gif-Sur-Yvette, France

A. Cavanna, G. Faini, U. Gennser, and D. Mailly
CNRS, phynano team, Laboratoire de Photonique et Nanostructures, Route de Nozay, F-91460 Marcoussis, France
(Received 15 October 2007; published 25 March 2008)

We have determined the finite temperature coherence length of edge states in the integer quantum Hall effect regime. This was realized by measuring the visibility of electronic Mach-Zehnder interferometers of different sizes, at filling factor 2. The visibility shows an exponential decay with the temperature. The characteristic temperature scale is found inversely proportional to the length of the interferometer arm, allowing one to define a coherence length l_φ. The variations of l_φ with magnetic field are the same for all samples, with a maximum located at the upper end of the quantum Hall plateau. Our results provide the first accurate determination of l_φ in the quantum Hall regime.

DOI: 10.1103/PhysRevLett.100.126802 PACS numbers: 73.43.Fj, 03.65.Yz, 73.23.Ad

The understanding of the decoherence process is a major issue in solid state physics, especially in view of controlling entangled states for quantum-information purposes. The edge states of the quantum Hall effect are known to present an extremely long coherence length l_φ at low temperature [1], providing a useful tool for quantum-interference experiments [2–6]. Surprisingly, very little is known on the exact value of this length and the mechanisms that reduce the coherence of edge states. This is in strong contrast with diffusive conductors, where weak localization gives a powerful way to probe l_φ. It has been shown, in this case, that electron-electron interactions are responsible for the finite coherence length at low temperatures. In the integer quantum Hall effect (IQHE) regime, the presence of a high magnetic field destroys any time reversal symmetry needed for weak localization corrections, making such an investigation difficult. Furthermore, due to the unidimensionality of the edge states, electron-electron interactions may strongly modify the single particle picture, and one can ask whether the notion of phase coherence length is still relevant and how it depends on temperature. In this Letter, we show for the first time that one can define a phase coherence length and that it is inversely proportional to the temperature.

Though the energy redistribution length has been studied in the past [7,8], these scattering experiments do not measure the phase coherence, which requires observation of electron interference effects. So far, experiments have only been able to put a lower bound on l_φ at low temperatures [2,9–11]. The electronic Fabry-Pérot interferences occurring in ballistic quantum dots have been used since the early days of mesoscopic physics [9]. These first studies showed an exponential decay of the amplitude of the Aharonov-Bohm (AB) oscillations with temperature [10]. However, this decay was attributed to thermal smearing due to the contribution of thermally activated one particle energy levels of the dot. Furthermore, the size of the interferometers was not varied, nor was a Fourier analysis performed of the AB oscillations that could yield an estimation of l_φ [12]. Quantum-dot systems also implicate the possible interplay of Coulomb blockade effects [13]. The Mach-Zender interferometers (MZI) [2,4,6] used in the present study do not suffer from the same limitations. First, we will show that the observed oscillations result from the interference of two paths of equal length, making thermal smearing negligible. Second, charge quantization effect leading to Coulomb blockade are irrelevant here. Last, comparison between MZI's of various sizes allows us the unambiguous determination of l_φ, as well as its dependence with temperature and magnetic field.

The sample geometry, presented in Fig. 1, is the same as in [6]. MZIs of different sizes were patterned using e-beam lithography on a high mobility two-dimensional electron gas formed at the GaAs/$Ga_{1-x}Al_xAs$ heterojunction (sheet density $n_S = 2.0 \times 10^{11}$ cm^{-2} and mobility $= 2.5 \times 10^6$ cm^2/V s). The experiments were performed in the IQHE regime at filling factor $\nu = n_S h/eB = 2$ (magnetic field $B \simeq 4.6$ T). Transport occurs through two edge states. Quantum point contacts (QPCs) $G0$, $G1$, and $G2$ define electronic beam splitters with transmissions $\mathcal{T}_i$ ($i =$ 0–2). In all the results presented here, the interferences were studied on the outer edge state schematically drawn as white lines in Fig. 1, the inner edge state being fully reflected by all the QPCs. The first gate $G0$ is tuned to fully transmit the outer ($\mathcal{T}_0 = 1$) edge state. The interferometer itself consists of $G1$, $G2$, and the small central Ohmic contact in between the two arms. $G1$ splits the incident beam into two trajectories (u) and (d), which are recombined with $G2$, leading to interferences. Samples have been designed such that (u) and (d) are of equal length. The sizes of the three interferometers used in this study scale by up to a factor of $\sqrt{2}$: the length of their arms are $L = 5.6$ μm, 8 μm, and 11.3 μm for enclosed areas of 8.5 μm^2 (referred to as "small"), 17 μm^2 ("medium"), and 34 μm^2 ("large"), respectively. The samples are cooled in a

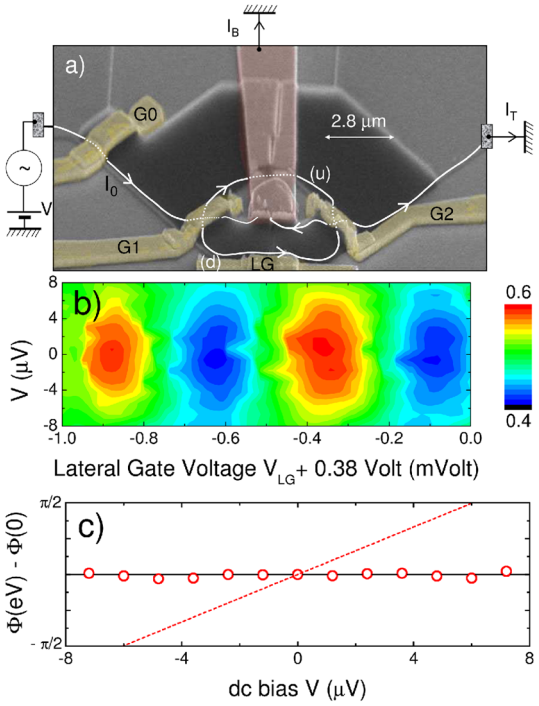

FIG. 1 (color online). (a) Tilted scanning electron microscope (SEM) view of the "small" MZI. $G0$, $G1$, and $G2$ are QPCs whose split gates are connected with gold bridges over an isolator responsible for the black color of the SEM view. LG is a lateral gate. The white line on the SEM picture represents the outer edge state. The small Ohmic contact in between the two arms collects the backscattered current I_B to the ground through a long gold bridge. (b) A 2D plot of dI_T/dI_0 as a function of the lateral gate voltage V_{LG} and the dc bias V, for the large sample at 20 mK. The visibility of interferences decreases with V while the phase of interferences remains almost constant. (c) Phase of the large sample deduced from Fig. 1(b). The dashed line is the energy dependence of the phase that would be necessary to explain our observed visibility decrease with thermal smearing.

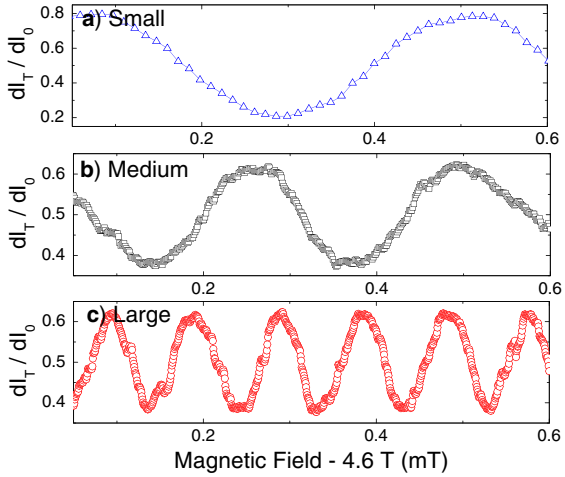

FIG. 2 (color online). Interferences revealed upon varying the magnetic flux through the surface defined by the two arms (u) and (d) of the interferometers. From the oscillation period δB we deduce the surface $S = h/(e\delta B)$ of the 3 different studied MZI. (a) The small MZI ($S = 8.7 \pm 0.2\ \mu\mathrm{m}^2$). (b) The medium MZI ($S = 15.5 \pm 0.4\ \mu\mathrm{m}^2$). (c) The large MZI ($S = 40.7 \pm 0.8\ \mu\mathrm{m}^2$). All these surfaces are in good agreement with the lithographic ones (see text).

dilution fridge to temperatures ranging from 20 mK to 200 mK.

The labels are indicated in the upper part of Fig. 1. A current I_0 is injected into the outer edge state through the interferometer. The current that is not transmitted, $I_B = I_0 - I_T$, is collected to the ground with the small central Ohmic contact. I_0 is made up of a minute ac part, with the possibility to superimpose a dc bias V. The differential transmission of the interferometer is defined as $\mathcal{T} = G/G_0 = dI_T/dI_0$, where $G = dI_T/dV$ is the differential conductance and $G_0 = e^2/h$. It is measured with a standard lock-in technique using a 619 Hz frequency and a 39 $\mathrm{pA_{rms}}$ amplitude ac bias. The corresponding bias voltage excitation (1 $\mu\mathrm{V_{rms}}$) is always smaller than the energy scale involved. The oscillations revealing the quantum interferences can be obtained using two equivalent experimental procedures: either by superimposing a minute current to the large current of the magnet or by changing the surface defined by the MZI using a lateral gate (LG). Figure 2 shows the AB oscillations of the transmission for the three interferometers, showing a magnetic period inversely proportional to the area of the interferometer, while Fig. 1(b) shows oscillations obtained using LG. After checking that both methods lead to the same interferences amplitude, we have always used the lateral gate and run the magnet in the permanent-current mode, strongly reducing the measurement noise. The visibility $\mathcal{V}$ of the AB oscillations is defined as the ratio of the half amplitude of the oscillation of the transmission divided by the mean value.

The maximum value of $\mathcal{V}$ is always obtained at the lowest temperature. $\mathcal{V}$ can reach 65% for the small interferometer, whereas it typically attains 20%–40% for the medium and the large interferometers [see Fig. 1(b)]. For each MZI we have studied the temperature dependence of the visibility. In Fig. 3, we have plotted $\ln(\mathcal{V}/\mathcal{V}_B)$ versus temperature, where $\mathcal{V}_B$ stands for the visibility at $T_B = 20$ mK. Clearly, the visibility decreases with temperature in all cases, and the larger the MZI, the stronger the temperature dependence. More quantitatively, if a linear regression of $\ln(\mathcal{V}/\mathcal{V}_B) = (T - T_B)/T_\varphi$ is done, one finds that T_φ^{-1} is proportional to the length of the interfering arms (inset of Fig. 3). In the following, we show that this behavior does not result from a thermal smearing.

The transmission probability through the MZI at the energy ϵ is $\mathcal{T}(\epsilon) = \mathcal{T}_1\mathcal{T}_2 + \mathcal{R}_1\mathcal{R}_2 + z\sqrt{\mathcal{T}_1\mathcal{R}_2\mathcal{R}_1\mathcal{T}_2} \times \sin[\phi(\epsilon)]$, where $z \in [0, 1]$ is a parameter accounting for phase averaging and/or decoherence, and $\mathcal{T}_i = |t_i|^2 = 1 - \mathcal{R}_i$ are the beam splitters' transmissions [14,15]. $\phi(\epsilon)$ is the AB flux across the surface $S(\epsilon)$ defined by the energy dependent edge state positions in the two inter-

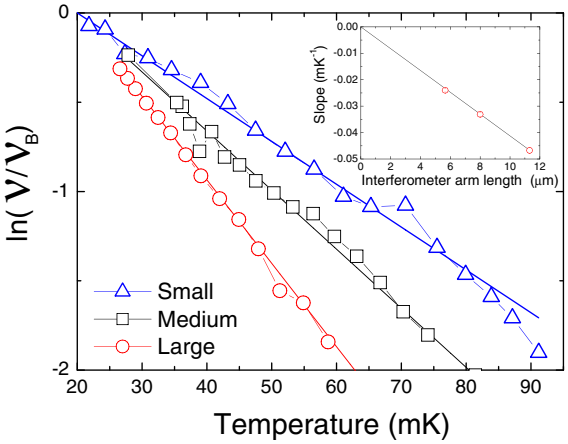

FIG. 3 (color online). $\ln(\mathcal{V}/\mathcal{V}_B)$ versus temperature for the three samples, $\mathcal{V}_B$ is the visibility measured at $T_B = 20$ mK. The measurement has been done at the magnetic field for which the visibility decay is the smallest. Inset: The slope $T_\varphi^{-1} = \ln(\mathcal{V}/\mathcal{V}_B)/(T - T_B)$ is proportional to the arm length.

fering arms, $\phi(\epsilon) = 2\pi S(\epsilon)eB/h$. When there is a finite length difference $\Delta L = L_u - L_d$ between the two arms, the surface S depends on the energy ϵ. Thus the phase varies with the energy, $\phi(\epsilon + E_F) = \phi(E_F) + \epsilon/(k_B T_S)$, where $k_B T_S = \hbar v_D/\Delta L$ [15] and v_D is the drift velocity (10^4 to 10^5 ms^{-1}) [16]. The differential conductance G at bias V and at temperature T probes the transmission probability at energy eV smeared over an energy range $k_B T$ [15]: $G(V) = G_0 \int_{-\infty}^{+\infty} f'(\epsilon)\mathcal{T}(\epsilon + \mathrm{eV})d\epsilon \propto \{1 + \mathcal{V}_0 < \sin[\phi(\mathrm{eV})] >_{k_B T}\}$, where $f'(\epsilon)$ is the derivative of the Fermi distribution. The energy dependence of the phase ϕ leads to a thermal smearing at finite temperature as the phase is blurred. A complete calculation yields a visibility decreasing like $\mathcal{V} = \mathcal{V}_0 \pi T/[T_S \sinh(\pi T/T_S)]$ [15]. In order to fit the visibility decrease with thermal smearing, this requires that $T_S \sim 66$, 59, and 44 mK, for the small, medium, and large sample, respectively [17].

On the other hand, at low temperature, T_S can be determined by measuring the phase of the interferences as a function of the dc bias V: $\phi(\mathrm{eV}) = \phi(0) + \mathrm{eV}/(k_B T_S)$. In Fig. 1(b) we have plotted a 2D graph of the differential transmission $\mathcal{T}(V)$ as a function of the lateral gate voltage and the dc bias, for the large sample at 20 mK. From this measurement we have deduced the phase $\phi(\mathrm{eV})$, which is shown to remain almost constant over an energy range of ~ 16 μeV [Fig. 1(c)]. As a comparison, the dashed line of [Fig. 1(c)] is the phase dependence that would be required ($T_S = 44$ mK) to explain the decrease of the visibility with thermal smearing. The conclusion is straightforward: our sample does not suffer from thermal smearing. We have done the same procedure for all the three samples, which exhibits a phase rigidity over at least ~ 16 μeV, meaning that all our samples have negligible thermal smearing in the explored temperature range $k_B T < 16$ μeV $\equiv$ 200 mK. One can notice that phase rigidity with the same order of energy range has been also observed in Ref. [18], on similar MZI [19].

The exponential decrease of the visibility with temperature is robust against various parameter variations, revealing a universal behavior. While the maximum visibility at the lowest temperature is affected by varying the transmissions $\mathcal{T}_i$ of the MZI and by applying a finite bias [6], T_φ^{-1} is found to be unaffected. In practice, the results presented here have been obtained with $\mathcal{T}_1 \sim \mathcal{T}_2 \sim 1/2$ and zero bias.

Indeed, and this is the central result of our Letter, our measurements can be interpreted by the introduction of a coherence length $l_\varphi(T)$ such that

$$\mathcal{V} = \mathcal{V}_0 e^{-2L/l_\varphi} \quad \text{with} \quad l_\varphi \propto T^{-1} \tag{1}$$

as shown in Fig. 3. $\mathcal{V}_0$ contains the temperature independent part of the visibility. In the inset of Fig. 3, we have plotted the slope $\mathcal{T}_\varphi^{-1}$ for the three samples [20]. It is clear that the slope scales with the length of the interferometer arm defining, *de facto,* a coherence length $l_\varphi(T)$ of about 20 μm at 20 mK. The magnetic field variation of the deduced l_φ is independent from the MZI size (see Fig. 4). In order to compare the three samples at the same filling factor, we have shifted the x axis of Fig. 4 by $+0.25$ T and -0.1 T for the small and large MZI, respectively. These values center the Hall plateaus all together. The maximum of the coherence length is reached at the upper

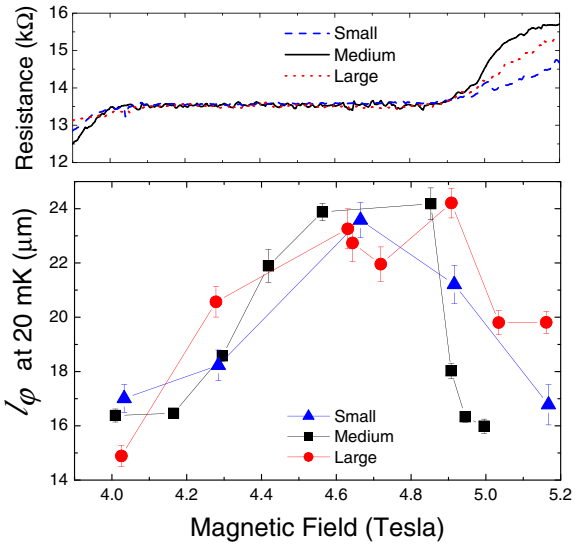

FIG. 4 (color online). Upper panel: The dashed, solid, and dotted lines are the two point Hall resistance at $\nu = 2$ measured for the small, the medium, and the large sample, respectively. l_φ has a general shape recovered by all three samples, with a maximum at the end of the Hall plateau. Lower panel: Coherence length at $T_B = 20$ mK, $l_\varphi = 2L.T_\varphi/T_B$ for the three samples studied ($L = 5.6$, 8, and 11.3 μm). The magnetic fields (x axis) of the small and large sample have been shifted by $+0.25$ and -0.1 T, respectively, such that the plateau centers coincide.

end of the plateau where the longitudinal resistance is usually minimum. However, our sample configuration does not allow us to check if it is actually the case.

Let us now compare our results with previously available data from other groups. Although the variations of $\mathcal{V}(T)$ were measured only for one interferometer size in the following experiments, it is possible to fit the data with Eq. (1) and to deduce a coherence length value at 20 mK. In the Fabry-Pérot type interferometer [Fig. (5b) of Ref. [10]], our analysis, using l_φ instead of thermal smearing, leads to $l_\varphi \sim 20$ μm at 20 mK. Although these experiments were performed with different filling factor, magnetic field, mobility, density, and geometry, surprisingly it gives the same result. The data from Ref. [2] yields also a similar l_φ, although a direct comparison is difficult without an exact knowledge of the MZI dimensions. Finally, the results of Ref. [4], again interpreted by the authors as resulting from thermal smearing, lead to $l_\varphi \sim 80$ μm at 20 mK.

What kind of mechanism is responsible for a finite coherence length varying with a T^{-1} temperature dependence? Electron-electron collisions are known to limit the coherence in non-unidimensional conductors (2D electron gas, diffusive metallic conductors). For the MZI, a finite l_φ coming from short range interaction ($l_\varphi \propto T^{-3}$), long range interaction [$l_\varphi \propto T^{-1}\ln^2(1/T)$], or curvature of the fermion dispersion ($l_\varphi \propto T^{-2}$) [21] cannot explain our findings. Alternatively, interactions with environment electrons, capacitively coupled to the arms of the interferometer, have been proposed to describe the decoherence of MZIs [22]. More specifically, decoherence is due to the thermal noise of the dissipative part of the finite frequency coupling impedance between the environment and the reservoirs. This theory leads to

$$\frac{l_\varphi}{L} = \frac{\tau_\varphi}{\tau} = \frac{\hbar}{2\pi k_B T}\frac{v_D}{L}, \qquad (2)$$

when $\pi\hbar C v_D/(Le^2) \ll 1$, C being a geometric capacitance, which represents the coupling to the environment and τ being the time of flight. For $v_D = 5.10^4$ ms^{-1} and $C/L \sim \epsilon_r\epsilon_0$, one finds $\pi\hbar C v_D/(Le^2) \ll 1$ and $l_\varphi \sim 3$ μm at 20 mK. This result agrees rather well with our measurements, although in the absence of an independent determination of v_D and C, it is not possible to be more quantitative. Moreover, the theory was developed for nonchiral wires coupled to a perfect conductor [22]. Also, one may ask what role may play the chirality and the environment of a nonperfect conductor.

We now turn to the nonmonotonic dependence of l_φ with the magnetic field B. If τ_φ is independent of B, as suggested by Eq. (2), the apparent variation of l_φ results from a variation of τ. As we have deduced l_φ assuming a constant trajectory length $l = L$, any variation of l, due to disorder, would modify the deduced $l_\varphi = \tau_\varphi L \times v_D/l$. Then, the maximum of l_φ shown in Fig. 4 corresponds to the minimum of l/v_D. In a naive picture, the drift velocity v_D varies like $1/B$ [16,23] barely leading to nonmonotonic variations of l_φ. On the other hand, a nonmonotonic variation of l is all the more plausible. The maximum of l_φ occurs on the upper end of the Hall plateau where one expects minimum backscattering, thus a minimum l. Assuming this explanation is correct, the overlap of the three curves in Fig. 4 (lower panel) indicates that the variations of l scale with the geometric length of the MZI. The study of the influence of the sample disorder on l_φ and its dependence with magnetic field could bring new insights supporting our assumption.

In conclusion, we have measured the visibility of Mach-Zehnder interferometers of various sizes, operating in the IQHE regime at filling factor 2, as a function of both the temperature and the magnetic field. Our results provide a direct and reliable measurement of the coherence length found to be inversely proportional to the temperature and maximum at the upper end of the Hall plateau. The order of magnitude is compatible with theoretical predictions based on a dephasing arising from the thermal noise of the environment.

[1] T. Martin and S. Feng, Phys. Rev. Lett. **64**, 1971 (1990).
[2] Y. Ji *et al.*, Nature (London) **422**, 415 (2003).
[3] P. Samuelsson, E. V. Sukhorukov, and M. Büttiker, Phys. Rev. Lett. **92**, 026805 (2004).
[4] L. V. Litvin *et al.*, Phys. Rev. B **75**, 033315 (2007).
[5] I. Neder *et al.*, Nature (London) **448**, 333 (2007).
[6] P. Roulleau *et al.*, Phys. Rev. B **76**, 161309(R) (2007).
[7] B. W. Alphenaar, P. L. MacEuen, R. G. Wheeler, and R. N. Sacks, Phys. Rev. Lett. **64**, 677 (1990).
[8] T. Machida *et al.*, Solid State Commun. **103**, 441 (1997).
[9] B. J. van Wees *et al.*, Phys. Rev. Lett. **62**, 2523 (1989).
[10] J. P. Bird *et al.*, Phys. Rev. B **50**, 14983 (1994).
[11] I. Yang *et al.*, Phys. Rev. B **71**, 113312 (2005).
[12] A. E. Hansen *et al.*, Phys. Rev. B **64**, 045327 (2001).
[13] B. Rosenow and B. I. Halperin, Phys. Rev. Lett. **98**, 106801 (2007).
[14] F. Marquardt and C. Bruder, Phys. Rev. B **70**, 125305 (2004).
[15] V. S.-W. Chung, P. Samuelsson, and M. Büttiker, Phys. Rev. B **72**, 125320 (2005).
[16] R. C. Ashoori *et al.*, Phys. Rev. B **45**, R3894 (1992).
[17] These T_S's would imply ΔL's incompatible with the lithography precision: 5, 6, and 8 μm from small to large MZI (taking $v_D = 5.10^4$ ms^{-1}).
[18] I. Neder *et al.*, Phys. Rev. Lett. **96**, 016804 (2006).
[19] The exact origin of the phase rigidity is still under debate.
[20] These slopes are the minimum values obtained at different magnetic fields. From small to large MZI: 4.41 T, 4.91 T, and 4.85 T.
[21] J. T. Chalkers, Y. Gefen, and M. Y. Veillette, Phys. Rev. B **76**, 085320 (2007).
[22] G. Seelig and M. Buttiker, Phys. Rev. B **64**, 245313 (2001).
[23] C. W. J. Beenakker, Phys. Rev. Lett. **64**, 216 (1990).